

# EMERGENT Project: Chipless Multisensor Rfid for GrEen NeTworks

G. Manara, *Fellow IEEE*, F. Costa  
*Member IEEE*, S. Genovesi, *Member IEEE*, S. Terranova, Francesco Alessio  
 Dicandia, Michele Borgese  
 Dipartimento Ingegneria  
 dell'Informazione  
 Università di Pisa  
 Pisa, Italy  
 g.manara@unipi.it

Lorenzo Monti, Luca Boggioni  
*Cubit scarl*  
 Polo Tecnologico di Navacchio, Via  
 Mario Giuntini, Navacchio  
 Pisa, Italy  
 luca.boggioni@cubitlab.com

A.Lazaro, *Senior Member IEEE*,  
 R.Villarino, D. Girbau, *Senior Member IEEE*  
 Electronics, Electrical and Automatics  
 Engineering Department  
 Universitat Rovira i Virgili (URV)  
 Tarragona, Spain  
 antonioramon.lazaro@urv.cat

Albert Escala  
*Generation RFID s.l.*  
 Carrer del Camí de Valls, 81, Reus  
 Tarragona, Spain  
 aescala@generationrfid.com

S. Tedjini, *Senior Member IEEE*, E.  
 Perret, *Senior Member IEEE*, Hatem El  
 Matbouly  
 University of Grenoble-Alpes  
 Grenoble INP, Laboratory LCIS  
 Valence, France  
 smail.tedjini@lcis.grenoble-inp.fr

Christophe Mercier, Pascal Pierron  
*Ardeje*  
 4 Rue Georges Auric, 26000  
 Valence, France  
 mercier@ardeje.com

**Abstract**—This work summarizes the main outcomes of the EMERGENT project that was mainly focused on the design of chipless RFID sensors and their realization on green substrates. Three different sensors are presented for monitoring humidity, temperature and breathing.

**Keywords**—Chipless RFID, chipless RFID sensor, frequency selective surface, radar cross section.

## I. INTRODUCTION

EMERGENT project lasted from January 2014 to December 2018. The project aimed to realize a class of chipless Radio Frequency IDentification (RFID) tags and sensors capable of enabling the next generation of pervasive Radio Frequency (RF) interconnected systems. To this aim, environmental-friendly substrates, such as paper, and low-cost fabrication processes, such as desktop inkjet printing, have been employed. Moreover, EMERGENT targeted also the realization of a dedicated reader necessary for extracting the desired information from the electromagnetic footprint of the tag/sensor. Chipless sensors are an effective extension of the concept of chipless tags but in order to acquire the sensing capability, the physical structure of the chipless device must be functionalized with an “active” material which is sensitive to the parameter to be sensed. In fact, the variation of the parameter to measure is transduced into a variation of the permittivity and/or the conductivity of the “active” material used for sensing.

The research activity carried out on tag and sensors has been multidisciplinary and subject to a continuous assessment by testing in a controlled environment as well as measured in operative environment. Research on chemical interactive materials (CIM) able to sense a change in a physical quantity and transduce it into an RF-measurable was addressed and required the development of suitable instrumentations and measurement procedures. In this sense, prototypes of small and medium chambers with controlled humidity have been fabricated, setups for variable-temperature conditions have been investigated. Dedicated

readers for passive and semi-passive chipless RFIDs have been developed as well.

Thanks to the consortium background and knowledge on the chipless RFID field [1]–[10], EMERGENT finally succeeded in designing, manufacturing and testing different kinds of wireless passive and semi-passive chipless smart tags and sensors able to sense the changing of a physical quantity in the surrounding environment. Among the many outcomes obtained by the joint effort of the involved universities and companies, this paper summarizes the achieved results for sensors of temperature and humidity as well as a breathing sensor [11].

## II. HUMIDITY SENSOR

The chipless RFID sensor for humidity has been realized by using a commercial desktop inkjet printer and employs a conductive silver ink does not require any specific curing in oven. The ink is deposited on a special paper which acts as a transducer of the humidity level of the external environment into a variation in the frequency response of the chipless RFID tag. The frequency shift has been demonstrated to be as high as 270 MHz without requiring any precise recovering of the RCS value. The reading system comprises only a single antenna operating in linear polarization within the bandwidth 2-8 GHz. The sensor is provided with a ground plane (GP), which improves the quality factor of the employed resonator. In addition, the GP allows the sensor to be placed on objects, even metallic ones, without any detuning effect of the frequency response of the tag.

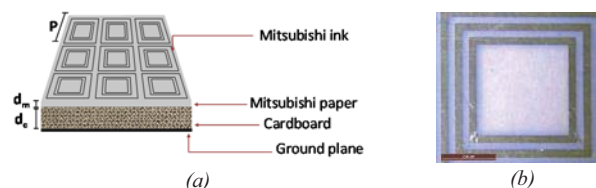


Fig. 1 Stack-up of the chipless sensor and layout of the resonant element (a) and a stereomicroscope image of the printed chipless tag (b). The scale bar is 200  $\mu\text{m}$ . The microscope adopted in this work is a Leica M165C.

This work was supported by EMERGENT under H2020 Grant Agreement 645771.

The fabricated prototype consists of 3x3 Frequency Selective Surface (FSS) elements placed on a grounded cardboard substrate (Fig.1a). The unit cell ( $P = 15$  mm) consists of a three-loop FSS printed on a thin paper sheet ( $d_m = 150$   $\mu\text{m}$ ) and placed on a thick grounded cardboard layer ( $d_c = 3$  mm) characterized by a permittivity  $\epsilon_r = 2.4 - j0.2$  (Fig1b). The reason of designing the resonant element as a periodic surface lays in the level of the backscattered signal which is directly proportional to the area of the tag. The repetition of the resonator on the plane allows to greatly improve the reading robustness, that is reducing the probability of error, and also extend read range.

After carrying out the measurements and the post processing stage, it is possible to link the variation of the RH level in the dedicated climatic chamber to the variation of the electromagnetic response of the proposed chipless RFID tag. The frequency responses of the tag measured for RH levels, equals to 50%, 70%, 80% and 90% are shown in Fig. 2 It is evident that the tag response exhibits 3 deep nulls at the frequencies of 3.076 GHz, 5.888 GHz and 7.275 GHz when RH=50% (minimum RH level achievable in the climatic chamber). By increasing the RH level inside the box, a downshift of the resonance peaks for the three frequencies is visible. This is due to the fact that the paper absorbs the moisture inside the climatic chamber and increases its electrical permittivity. Consequently, the resonant frequencies of the printed tag decrease. The higher the RH level the greater the downshift of the frequency response of the tag.

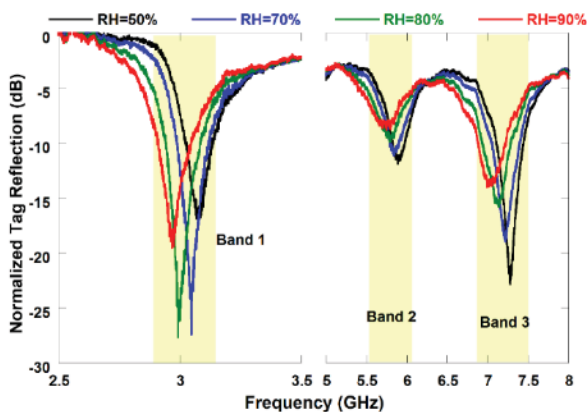


Fig. 2 Normalized reflection coefficient measurement of the chipless tag for different humidity levels.

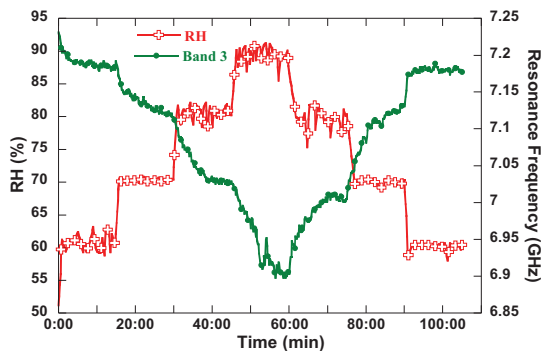


Fig. 3 Comparison between the RH level and the third resonance frequency.

It is worthwhile to mention that the process is completely reversible since once the tag is dried with warm air, the frequency response of the tag returns to its initial state (Fig. 3). It is therefore possible to conclude that the tag is able to absorb and release humidity with a reversible process.

### III. CHIPLESS TEMPERATURE THRESHOLD SENSOR

Chipless temperature sensing is a topic of recent interest in RFID research community. Different structures have been realized and tested [19 - 22]. However, reading chipless tags have many constraints concerning the usage of reading impulses, which do not exist in commercial readers. The challenge in this work is to design a solution based on standard RFID system to read chipless sensor-tags. The idea is to use resonant structures as a passive chipless wireless sensor that can be interrogated using commercial RFID readers for threshold temperature information in dual commercial frequency bands. The sensor operating principle is based on encoding temperature ranges in a binary format using two C-like resonators (Fig. 4). The two resonators are designed on a temperature sensitive dielectric substrate where one resonator resonates in the ETSI UHF RFID band, while the other resonator resonates in 2.4 GHz ISM band. Temperature variation introduces a shift in the position of the resonance and anti-resonance peaks of the Radar Cross Section (RCS) of the backscattered signal. Depending on the position of the peaks, the power level of the scattered signal shifts from maximum which corresponds to (logic '1') to minimum, which corresponds to (logic '0'). Using this coding, the temperature range information is encoded as 2 bits value.

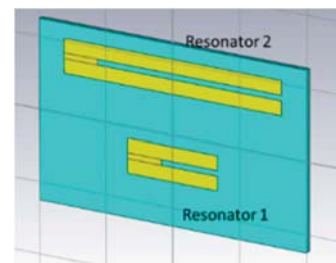


Fig. 4 Temperature sensor structure based on the two C-like resonators on temperature sensitive substrate.

As apparent from Fig. 4, the structure of the proposed temperature sensor consists of two C-like resonators on a temperature sensitive dielectric substrate. Resonator 1 has a resonance frequency of 0.862 GHz while resonator 2 has a resonance frequency of 2.43 GHz. The choice of these frequencies is made in order for the proposed sensor to be used in commercial allocated frequency bands (ETSI & ISM bands). The operation principle is based on a resonance frequency shift of RCS peak due to the permittivity variation as a function of temperature. The substrate has been chosen to have high dielectric constant for sensor size reduction as well as high coefficient of dielectric constant for significant frequency shift under temperature variation. To study the effect of temperature variation on the backscattered RCS frequency shift, the structure has been simulated with substrate parameters ( $\epsilon_r = 30$ ,  $h = 1$  mm,  $\tan\delta = 0.001$ ) and coefficient of dielectric constant of  $-370 \times 10^{-6}/^\circ\text{C}$ .

Simulation results show that C-like scatter exhibits a resonant frequency and an anti-resonance frequency. The specific geometry of the C-like allows obtaining resonance of an open/shorted structure leading to  $\lambda/4$  resonator. It is worth noting that the same configuration shows an anti-resonance frequency slightly different. In the proposed design we exploit the resonant frequency as the RCS level associated to that frequency is more suitable for detection and therefore practical implementation of the measurement. Simulation results show that the corresponding resonance peak shifts under different temperature values.

The two C-like scatters act as two bits encoder for a temperature range. Logic ‘1’ is represented by a resonance lies within the band, while logic ‘0’ is represented by a resonance outside the band. The encoding depends on the band width and the amount of resonance shift due to temperature variations. Since the ETSI and ISM bands do not have the same band width, one expects that the resonance shift will not be the same and hence allowing different combination of binary code to be assigned to ranges of temperatures. The ranges of temperatures in the ETSI band and in the ISM band are reported in Fig. 5.

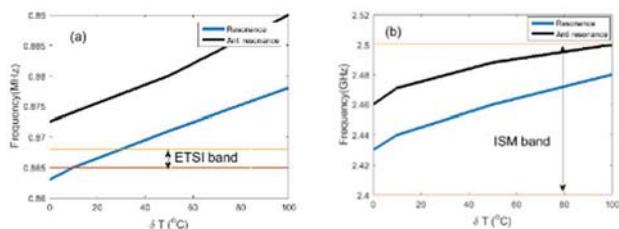


Fig. 5 Simulated resonance frequency shift due to temperature variation from 0 to 100 °C (a) for the 0.862 GHz peak. (b) for 2.43 GHz peak

Measurements have been performed on manufactured chipless RFID sensors. The sensor prototype is placed on a temperature controlled hot plate. At any moment during the interrogation, the temperature of the sensor prototype is measured using infrared thermometer. The measurement starts by measuring the background reflection from the environment without introducing the sensor prototype. Then the sensor is introduced on the hotplate at 20 cm from the interrogation antenna. The backscattered signal from the sensor prototype is received through the reader antenna and it is subtracted from the background reflection measured previously.

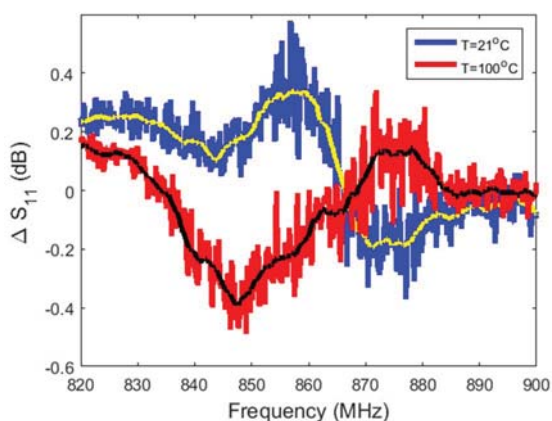


Fig. 6 Measured backscattered power at different temperatures.

The results of the S parameters measured at two different temperatures first at room temperature (21 °C) and at (100°C) are illustrated in Fig. 6. By comparing the two measurements, there is a peak shift at 100°C with respect to the room temperature measurement of about 16 MHz. This result is shown as an example for concept proof, less resonance shift can be achieved either by using the substrate dielectric material or applying less temperature difference.

#### IV. WEARABLE BREATHING SENSOR BASED ON MODULATED FREQUENCY SELECTIVE SURFACES

Commercial breathing sensors often use data loggers in order to store measurements, which can be processed after downloading their data onto a computer. Recently, vital-sign monitoring using Doppler radar or UWB radar has been investigated in the literature. However, although these approaches are not invasive but are sensitive to body movements [12]. Unlike those sensors, the system presented in this work allows real-time wireless measurements [13] [14]. The real-time capability allows continuous monitoring of critical patients in hospitals, for which an alarm can be activated when the patient stops breathing. Since the backscattering communication is employed, the transponder does not need any transmitter (e.g. Bluetooth). Furthermore, the integrated circuitry in the transponder draws low power consumption, since no ADC or microcontroller is required. Since the battery only feeds the oscillator, a large reduction in terms of power consumption is obtained. Consequently, the battery lifetime is enough high allowing the system works continuously. The continuous monitoring is usually performed in the case of apnea diagnosis, where several days of analysis are required. The proposed system is shown in Fig. [13] [14]. As a proof of concept, a custom reader has been designed with commercial components for wireless measurements. The reader illuminates the transponder with an unmodulated CW at 2.45 GHz ( $f_c$ ). The transponder backscatters the wave from the reader and modulates the incoming signal at the frequency of the oscillator (see Fig. 7), which depends on the temperature of the air [13] [14]. The transponder is a modulated Frequency Selective Surface (FSS). This is made of dipoles loaded with low-cost silicon varactors (Skyworks SMV1247-079LF) that are used as switching diodes [15] [16]. The varactor-loaded FSS is integrated into a headband along with the oscillator and the battery, as shown in Fig. 8. The FSS is implemented using a 100  $\mu\text{m}$ -thick flexible substrate (Rogers Ultralam 3850). The NTC is connected with thin flexible wires to the oscillator to reduce the interaction with the skin, which would be more comfortable for the patient. The oscillator, based on the two-inverter that is introduced here, draws 40  $\mu\text{A}$  at 3V; this leads to more than one year in the lifetime of a typical 330 mAh coin-battery. In addition, this solution allows miniaturization of the device, as the number of parts in the system is decreased.

Fig. 9 shows an example of the spectrum at 1.6 m and 4.8 m, and the measured received power as a function of the distance [15]. Read range higher than 3 m can be obtained in real environments with NLOS propagation [16]-[17]. The sensor temperature depends on the NTC resistance R and it

can be determined from the modulation frequency ( $f_m=0.455/RC$ ) [13].

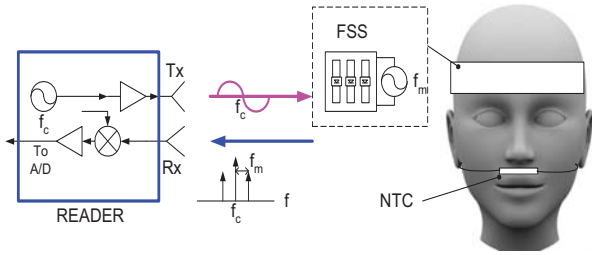


Fig. 7 Block diagram of the system, including the reader and the transponder

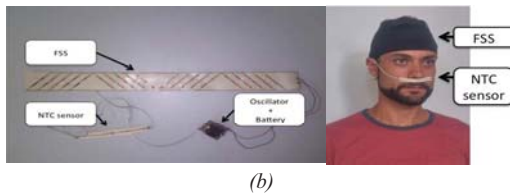
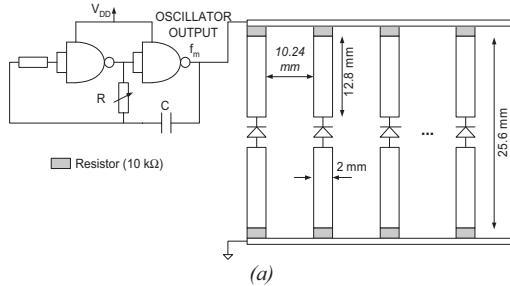


Fig. 8 Schema (a) and photography (b) of a FSS loaded with varactors connected to the two-inverter oscillator controlled by the NTC resistance (R).

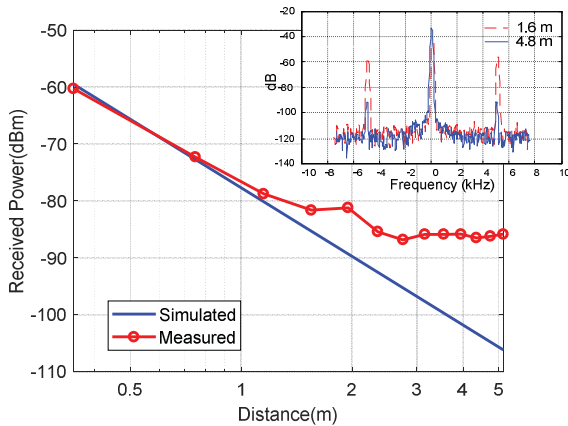


Fig. 9 Measured received power as function of read distance and comparison with simulated free space model.

The modulation frequency can be obtained from the spectrum of the base band signal at the output of the mixer which is digitalized with a PC sound card. The chirp Z-transform (CZT) algorithm and a Hamming window is used to achieve the appropriated frequency resolution. The modulation frequency  $f_m$  is estimated from the peak of CZT using 1000 samples taken with the ADC at 44000 Hz. This procedure (sampling plus CZT and Peak detection) needs approximately 63 milliseconds. As a result, the modulation frequency that is a function of the breathing is sampled at approximately 15 Hz. This sampling frequency is enough

because a normal breathing rate is around 0.3 Hz. Fig.10 shows an example of measurement of the breathing rate with an apnoea period in the middle [13] [14].

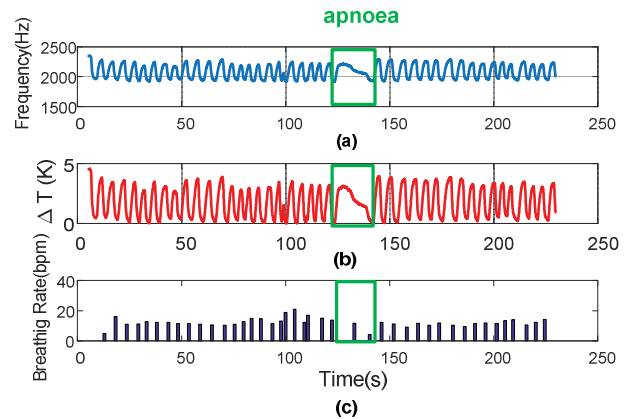


Fig. 10 Example of measurement for a person with an apnoea period: (a) measured modulation frequency, (b) temperature change and (c) breathing rate in bpm as function of the time

## V. CONCLUSIONS

An overview of the results of the EMERGENT project have been presented. In particular, three sensors prototypes realized with passive and semi-passive chipless RFID tags have been described and their performance assessed. More details on the developed technologies and methods will be provided at the conference.

## REFERENCES

- [1] F. Costa, S. Genovesi, and A. Monorchio, "A Chipless RFID Based on Multiresonant High-Impedance Surfaces," *IEEE Transactions on Microwave Theory and Techniques*, vol. 61, no. 1, pp. 146–153, Jan. 2013.
- [2] A. Vena, E. Perret, and S. Tedjini, "Chipless RFID Tag Using Hybrid Coding Technique," *IEEE Transactions on Microwave Theory and Techniques*, vol. 59, no. 12, pp. 3356–3364, Dec. 2011.
- [3] A. Ramos, E. Perret, O. Rance, S. Tedjini, A. Lazaro, and D. Girbau, "Temporal Separation Detection for Chipless Depolarizing Frequency-Coded RFID," *IEEE Transactions on Microwave Theory and Techniques*, vol. 64, no. 7, pp. 2326–2337, Jul. 2016.
- [4] M. Borgese, F. A. Dicandia, F. Costa, S. Genovesi, and G. Manara, "An Inkjet Printed Chipless RFID Sensor for Wireless Humidity Monitoring," *IEEE Sensors Journal*, vol. 17, no. 15, pp. 4699–4707, 2017.
- [5] A. Vena, E. Perret, and S. Tedjini, "Design of Compact and Auto-Compensated Single-Layer Chipless RFID Tag," *IEEE Transactions on Microwave Theory and Techniques*, vol. 60, no. 9, pp. 2913–2924, Sep. 2012.
- [6] A. Ramos, D. Girbau, A. Lazaro, and R. Villarino, "Wireless Concrete Mixture Composition Sensor Based on Time-Coded UWB RFID," *IEEE Microwave and Wireless Components Letters*, vol. 25, no. 10, pp. 681–683, Oct. 2015.
- [7] S. Genovesi, F. Costa, A. Monorchio, and G. Manara, "Chipless RFID Tag Exploiting Multifrequency Delta-Phase Quantization Encoding," *IEEE Antennas and Wireless Propagation Letters*, vol. 15, pp. 738–741, 2016.
- [8] F. Costa, S. Genovesi, and A. Monorchio, "Normalization-Free Chipless RFIDs by Using Dual-Polarized Interrogation," *IEEE Transactions on Microwave Theory and Techniques*, vol. 64, no. 1, pp. 310–318, Gennaio 2016.
- [9] R. S. Nair, E. Perret, S. Tedjini, and T. Baron, "A Group-Delay-Based Chipless RFID Humidity Tag Sensor Using Silicon Nanowires," *IEEE Antennas and Wireless Propagation Letters*, vol. 12, pp. 729–732, 2013.

- [10] A. Lazaro *et al.*, “Chipless Dielectric Constant Sensor for Structural Health Testing,” *IEEE Sensors Journal*, vol. 18, no. 13, pp. 5576–5585, 2018.
- [11] “<http://www.emergent-rise.eu/>.”
- [12] A. Lazaro, D. Girbau, and R. Villarino, “Techniques for clutter suppression in the presence of body movements during the detection of respiratory activity through UWB radars,” *Sensors (Basel)*, vol. 14, no. 2, pp. 2595–2618, Feb. 2014.
- [13] S. Milici, J. Lorenzo, A. Lázaro, R. Villarino, and D. Girbau, “Wireless Breathing Sensor Based on Wearable Modulated Frequency Selective Surface,” *IEEE Sensors Journal*, vol. 17, no. 5, pp. 1285–1292, Mar. 2017.
- [14] A. Lazaro, S. Milici, R. Villarino, and D. Girbau, “Wearable breathing sensor based on Modulated Frequency Selective Surfaces,” p. 4.
- [15] J. Lorenzo, A. Lázaro, R. Villarino, and D. Girbau, “Modulated Frequency Selective Surfaces for Wearable RFID and Sensor Applications,” *IEEE Transactions on Antennas and Propagation*, vol. 64, no. 10, pp. 4447–4456, Oct. 2016.
- [16] J. Lorenzo, A. Lazaro, D. Girbau, R. Villarino, and E. Gil, “Analysis of on-Body Transponders Based on Frequency Selective Surfaces,” *Progress In Electromagnetics Research*, vol. 157, pp. 133–143, 2016.
- [17] J. Lorenzo, A. Lazaro, R. Villarino, and D. Girbau, “Diversity Study of a Frequency Selective Surface Transponder for Wearable Applications,” *IEEE Transactions on Antennas and Propagation*, vol. 65, no. 5, pp. 2701–2706, May 2017.